Note: This is an original preprint version of a manuscript, and has not been peer reviewed. Data may be preliminary. The final peer-reviewed version of this article was published by Taylor & Francis in Hydrological Sciences Journal on 27/02/2026, and is available at: https://doi.org/10.1080/02626667.2025.2596270.

AUTHOR'S ORIGINAL MANUSCRIPT - PREPRINT

Fully non-contact discharge measurement in shallow streams via physics-based water-surface image analysis

Giulio Dolcetti[a], Farhad Bahmanpouri[b], Ashkan Pilbala[c]

[a]Department of Civil, Environmental and Mechanical Engineering, Università degli Studi di Trento, Trento, Italy; [b]The National Research Council (CNR) - Research Institute for Geo Hydrological Protection (IRPI), Perugia, Italy; [c]Department of Civil, Environmental and Architectural Engineering, University of Padova, Padua, Italy

ABSTRACT

Non-contact image-based velocimetry methods provide a flexible, cost-effective, and safe alternative to standard river discharge measurement techniques, but require prior knowledge of the bathymetry and suitable tracer distributions. Image wave velocimetry (IWV) approaches estimate the flow velocity and water depth simultaneously without artificial tracers, but have a low spatial resolution and lack robustness. Here, we extend a previous IWV approach to reconstruct the spatial transverse distribution of the surface velocity and depth across a river and determine the water discharge. We introduce a novel physics-informed approach that integrates the IWV analysis in an entropy-based framework, improving the resolution and robustness of the reconstructions. Testing in a shallow stream showed a 10% error in discharge for the extended IWV method, which improved to 4% with the combined IWV-entropy method. The results demonstrate the unprecedented capability of IWV methods to measure the discharge of shallow rivers without requiring any contact with water.

KEYWORDS

discharge; river monitoring; remote sensing; flow velocity; bathymetry

1. Introduction

Measuring river discharge, a key variable in the hydrological cycle, is a major task in hydrometry due to its significance in addressing various hydrological and geomorphological research questions. Traditional discharge measurement approaches require the immersion of an instrument in water, leading to increased risks for the instrumentation and for the operator. Small free-flowing streams, in particular, are usually unsuitable for fixed gauging systems and require traversing by foot to measure the flow velocity and water depth at multiple locations along a transect: a time-consuming and potentially very high-risk activity. Non-contact methods to measure rivers' flow rate and velocity have become an increasingly popular alternative to traditional intrusive methods thanks to their flexibility, rapid deployment, lower risk for the operators, and often lower costs. These methods use radar (Plant et al. 2005, Alimenti et al. 2020), acoustic (Dolcetti and Krynkin 2017, Dolcetti et al. 2017), or optical (Perks 2020, Jolley et al. 2021, Manfreda et al. 2024) signals to estimate the flow velocity at the water surface. This data is then combined with a known bathymetry and a hydraulic

Corresponding author: Farhad Bahmanpouri. Email:farhadbahmanpouri@cnr.it

model to quantify the water discharge.

Optical methods, in particular, use videos or image sequences of the water surface to reconstruct a quasi-instantaneous map of the surface velocity distribution across the river, enabling the accurate representation of relatively complex flow morphologies. The most common optical velocimetry approaches differ mostly in the image analysis approach: large-scale particle image velocimetry (LSPIV) (Fujita et al. 1998, Hauet et al. 2008, Peña-Haro et al. 2021) employs the spatial cross-correlation of image sub-windows across subsequent time-frames; large-scale particle tracking velocimetry (LSPTV) (Dal Sasso et al. 2018, Tauro et al. 2019, Perks 2020) tracks single features in a Lagrangian framework; space-time image velocimetry (STIV) (Fujita and Tsubaki 2002, Legleiter et al. 2024) is based on the average image space-time gradient produced by surface features; optical flow (OF) (Khalid et al. 2019, Ljubičić et al. 2024) tracks surface features according to a transport equation. The surface features can be floating tracers that are either naturally present (foam, leaves, etc.) or artificially added to the flow, or local variations in light intensity caused by water surface deformations (waves, ripples, or turbulent boils/vortices, e.g., Brocchini and Peregrine (2001)).

All optical velocimetry approaches mentioned above have two key common requirements: (i) surface features must be clearly visible and move approximately at the same velocity as the flow, and (ii) the water depth distribution must be known. The first requirement often mandates the artificial addition of tracers (seeding) (Dal Sasso et al. 2020). Passive tracers, such as leaves, floating particles, etc., are transported approximately at the same velocity as the flow near the surface. Instead, some water surface deformations, such as ripples and/or waves, propagate in various directions with a non-zero velocity relative to the mean flow speed, violating the first requirement. The error caused by waves is higher when the tracers' density is low (Tauro et al. 2014, Benetazzo et al. 2017), and can be as high as 100 %, depending on the image frame rate (Dolcetti et al. 2020). Advanced STIV algorithms include ways to filter out the effects of waves (Zhao et al. 2021), but still need a suitable tracer density distribution. The second requirement, i.e., the prior knowledge of the bathymetry, is probably one of the main challenges for the widespread adoption of non-contact optical velocimetry approaches. Variations in water level can be measured remotely using cameras (Young et al. 2015). However, the water depth may change, especially during floods, due to variations in the bed elevation. Through-water imaging (Woodget et al. 2015) has limited accuracy at larger depths due to light diffraction and becomes impossible in turbid waters. As a result, water depth measurements typically require physical access to the river by an operator or through a thawed or remotely controlled boat, defeating the purpose of non-contact methods.

Some recent scientific innovations show the potential to overcome these longstanding challenges. Legleiter and Kinzel (2021) employed a flow resistance equation to relate the measured surface velocity to the local water depth, enabling the simultaneous reconstruction of the velocity distribution and bathymetry based solely on LSPIV data. The approach looks very promising but has some limitations: the reconstruction requires a knowledge of the surface slope and of a hydraulic roughness coefficient, and is based on the assumption of a constant relationship between surface velocity and water depth at each location across the transect. Moreover, the LSPIV approach still requires the presence of passive tracers. A related approach based on microwave Doppler radar that does not require tracers has emerged recently as a suitable alternative (Chen et al. 2023).

Image Wave Velocimetry (IWV) techniques (Streßer et al. 2017, Dolcetti et al. 2022) have emerged as a new physics-based approach to overcome the limitations of existing optical velocimetry methods concerning both seeding and bathymetry knowledge requirements. These methods exploit the expected dependence of water wave celerity on flow velocity and water depth to estimate the velocity (Streßer et al. 2017) and/or the average water depth (Dolcetti et al. 2022) simultaneously. They do not require seeding but rely on the presence of gravity-capillary waves, which originate naturally due to the interaction of the water surface with wind (Miles 1957, Phillips 1957), with turbulence in water (Teixeira and Belcher 2006), or with the rough bed (Dolcetti et al. 2016, Dolcetti and García Nava 2019). In principle, IWV approaches enable a fully non-contact measurement of the flow rate in all conditions where the water surface has visible wave patterns, regardless of their forcing mechanism. In practice, however, the sensitivity of waves to variations in water depth is rather small and limited to long waves with a wavelength larger than the water depth. This results in a lack of robustness of the approach, leading to large uncertainties, especially in the water depth reconstruction. Robust results can be obtained only in relatively shallow rivers where the Froude number is larger than ~ 0.4 (Dolcetti et al. 2022), and the size of the image used for the analysis should be much larger than the water depth, at the expense of the spatial resolution.

In parallel, the entropy theory has emerged as an effective framework to reconstruct the cross-sectional velocity or water depth distributions in rivers based on a limited amount of data. The approach applies directly to the transverse distribution of the maxima of the velocity profile along the vertical direction (Chiu 1987, 1988). This makes the framework particularly suitable for non-contact measurement applications, since the maximum velocity is often found close to the water surface (Moramarco et al. 2004).

For instance, the entropy framework has been used to estimate the cross-sectional velocity distribution and discharge based solely on the surface velocity distribution (Bahmanpouri et al. 2022b, Rezazadeh et al. 2025), or on a single surface velocity measurement (Bahmanpouri et al. 2022a). By extending the entropy approach to the water depth distribution across a river transect (Moramarco et al. 2013), the shape of the bathymetry can be linked directly to the surface velocity distribution, enabling a non-contact bathymetry reconstruction through a single calibration parameter and with the prior knowledge of just the maximum water depth (Kechnit et al. 2024).

So far, bathymetry reconstructions based on IWV have been limited to the estimation of the spatially averaged water depth and have lacked robustness, while those based on the entropy theory require a site-specific calibration. The goal of this work, then, is to leverage the combined potential of both methods to overcome these limitations. We propose two possible solutions: the first one consists of a spatially-resolved extension of the IWV techniques that can reconstruct the water depth distribution along a transect, albeit with potentially large local errors; the second employs the entropy theory to provide a physically consistent constraint for the IWV-estimated bathymetry and velocity distribution, hence allowing a more realistic and potentially more accurate reconstruction of the flow discharge.

2. Materials and method

2.1. *Measurement site*

The field measurements were conducted on the Fersina river, a 26 km long, snowmelt-fed, 2nd order gravel bed river with its headwaters at 2005 m a.s.l., draining a 171 km^2

catchment, and joining the Adige River at 181 m a.s.l. in Trento, Trentino Province, Northeast Italy. The mean annual discharge of the Fersina is about 3 m^3/s (based on data from 2009). The measurements were carried out 9 km upstream from the joining point of Fersina and Adige rivers (46°04′53″N11°11′20″E) in June 2023, when flow discharge was lower, 1 m^3/s (Fig. 1).

Velocity profiles were measured along a 6.8 m wide transect using a hand-held acoustic velocity profiler (Hydroprofiler M-Pro). The instrument measures the vertical distribution of the time-averaged streamwise velocity component from a distance of 7 cm above the bed to a distance of 7 cm beneath the water surface, with a fine spatial resolution of 2 mm. It also measures the water depth, simultaneously. Its capability to measure in relatively close proximity to the bed and water surface makes it suitable for measurements in shallow depths. According to specifications, the instrument has an accuracy of 1% and a measuring range of ±0.25 cm/s for velocity measurements and 0.1% for depth measurements. The velocity profiles were recorded at a set of locations along the transect with horizontal separation of 0.5 m, and were repeated twice within one hour.

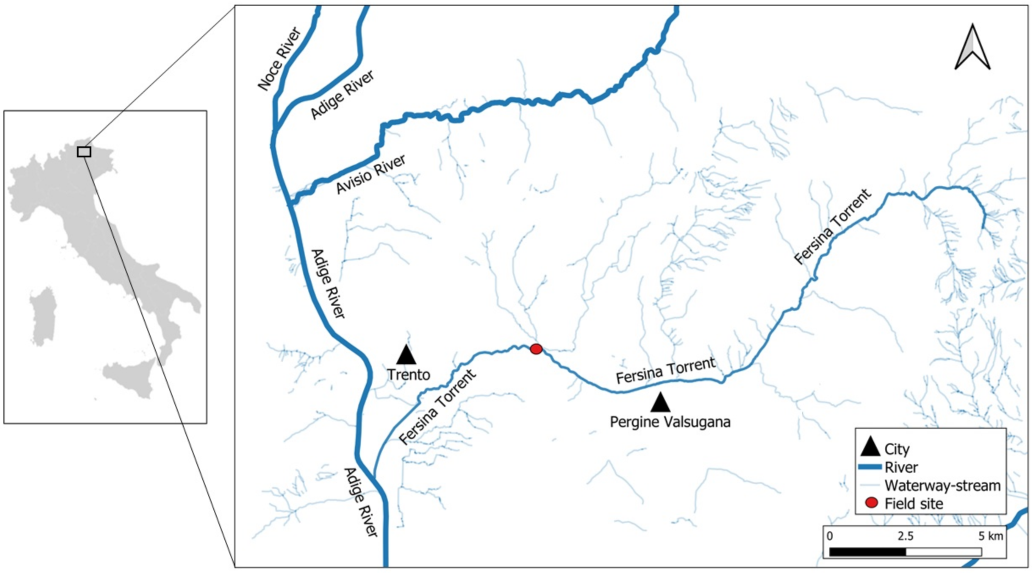

Figure 1. Map of Fersina stream in northern Italy, showing the location of the field monitoring site.

2.2. *Video-based surface and depth measurements*

IWV methods are well established in oceanography (e.g., Senet et al. (2001), Almar et al. (2021)), but they have been applied in rivers for the first time only recently. Streßer et al. (2017) first employed an IWV approach to map the velocity distribution in a large river, where the generation and dynamics of water waves were dominated by wind, as in the ocean. The method was then extended by Dolcetti et al. (2022), who demonstrated its application to simultaneously estimate velocity and water depth in shallow rivers, where waves originate due to the interaction of the sheared flow with the rough bed. Open-access software libraries based on the work of Dolcetti et al. (2022) have been created in Matlab (Dolcetti et al. 2023) and python (Dolcetti et al. 2024b), and the technique was recently applied also to non-contact acoustic imaging

(Dolcetti et al. 2024a).

The IWV approach applies a spatial-temporal Fourier analysis to sequences of images of the water surface to identify the water surface celerity. Each Fourier mode is uniquely identified by a frequency f and wavenumber $\boldsymbol{k} = (k_x, k_y)$ with modulus $|\boldsymbol{k}| = 2\pi/\lambda$, where λ is the wavelength and k_x and k_y are the components along the two horizontal co-ordinates x and y. The celerity of a mode with wavenumber $\boldsymbol{k}$ is $c(\boldsymbol{k}) = 2\pi f/|\boldsymbol{k}|$ directed along the same direction as $\boldsymbol{k}$, perpendicular to the wave crest.

It is generally observed that the surface of most rivers is deformed with various shapes and patterns, which are classified as either turbulence-forced patterns or gravity-capillary waves, based on their dynamics and mechanisms of generation (Brocchini and Peregrine 2001, Muraro et al. 2021). Turbulence-forced patterns represent surface deformations that are direct persistent manifestations of the interaction of turbulent structures with the water surface, such as turbulent boils, scars, or vortex dimples, which appear fixed or very slowly changing in a frame of reference moving with the flow (Dolcetti et al. 2016). As a result, their spectral signature has a frequency

$$f_t = \boldsymbol{k} \cdot \boldsymbol{V}/(2\pi), \tag{1}$$

which corresponds to a plane in the $(\boldsymbol{k}, f)$ space, where $\boldsymbol{V}$ is the flow surface velocity vector with modulus V. Patterns of natural or artificial tracers would also appear with frequencies along the same plane since they move with the same velocity as the flow.

In contrast, gravity capillary waves originate in most rivers due to forcing by wind, by turbulence in water, and/or by the pressure distribution on the rough bed, often resulting in relatively broad wave spectra dominated by the presence of stationary, or standing waves (Dolcetti et al. 2016, Dolcetti and García Nava 2019). Regardless of their generation mechanism, gravity-capillary waves propagate relative to the mean flow with a relative celerity $c_i(k) = 2\pi f_i/k$, where f_i is the intrinsic frequency,

$$f_i = \frac{k}{2\pi}\sqrt{gD\frac{(1+\mathrm{B})}{\mathrm{B}}\frac{\tanh(kD)}{kD}}, \tag{2}$$

D is the water depth, $\mathrm{B} = \rho g/\left(k^2\gamma\right)$ is the Bond number (the ratio of gravity and surface tension effects), g is the acceleration due to gravity, γ is the surface tension coefficient, and ρ is the water density. When the waves propagate on the surface of a vertically-sheared flow, the celerity varies depending on the velocity profile and surface wavelength. Let z represent the vertical coordinate such that $z = 0$ lies on the water surface and $z = -D$ lies on the riverbed, where D is the water depth. Approximating the flow velocity distribution U as a linear function of z,

$$U(z) = \left(m\frac{z}{D} + 1\right)V, \tag{3}$$

the frequency of gravity-capillary waves on a sheared flow can be calculated as (Biesel 1950)

$$f_w = [1 - \beta(k, D)]f_t \pm \sqrt{[\beta(k, D)f_t]^2 + f_i^2}, \tag{4}$$

where

$$\beta(k, D) = \frac{m}{2} \frac{\tanh(kD)}{kD}, \tag{5}$$

and $m = (D/V)(\mathrm{d}U/\mathrm{d}z)$ is a non-dimensional velocity gradient coefficient. m can be linked to the so-called velocity index α, i.e., the ratio between the depth-averaged velocity and the velocity at the surface, (Dolcetti et al. 2022)

$$\alpha = \frac{1}{VD} \int_{-D}^{0} U(z)\mathrm{d}z = 1 - \frac{m}{2}. \tag{6}$$

Equations 1 and 4 indicate a direct physical link between the flow surface velocity (V), water depth (D), and the surface frequency and wavenumber components of the surface spectrum that can be measured by a Fourier analysis (Dolcetti et al. 2022). Then, V and D can be estimated by fitting the measured discrete Fourier frequency-wavenumber spectrum of the surface with a theoretical spectrum that follows Eq. 1 and 4. This is achieved by finding the combination of V and D that maximises the so-called Normalised Scalar Product (NSP) between the measured Fourier spectrum $I(k_{x,p}, k_{y,q}, f_n)$ and the theoretical spectrum $S(k_{x,p}, k_{y,q}, f_n, V, D)$, where $k_{x,p}$, $k_{y,q}$, and f_n are a discrete set of wavenumbers and frequencies represented by the indices p, q, and n, respectively (the approach and procedure to build the theoretical spectrum are described in more detail by Dolcetti et al. (2022)).

So far, the application of the IWV approach to reconstruct the water depth has been limited to relatively shallow and fast flows, where the Froude number is subcritical but finite, $\mathrm{F} = V/\sqrt{gD} \geq 0.4$ (Dolcetti et al. 2022). The reason is twofold: on one hand, a relatively large Froude number is required for the generation of significant water surface deformations (Brocchini and Peregrine 2001); on the other hand, the change in wave frequency due to depth variations is extremely small when the Froude number is low (Dolcetti et al. 2022). As a result, the accuracy and resolution of the method depend both on the Froude number and on the size L of the image (Dolcetti et al. 2022). Given the small sensitivity of the wave dynamics to variations in water depth, the water depth can only be estimated accurately when L is large compared to the depth itself, since the minimum detectable variation in wavenumber scales with $2\pi/L$. Therefore, for the only known application of IWV methods to measure river discharge, Dolcetti et al. (2022) applied the analysis to a single large window covering almost the entirety of the river width. However, this may result in a potentially large bias if the velocity and depth vary horizontally over a distance smaller than L (Weichert et al. 2024).

2.3. *Entropy theory*

The application of a probabilistic entropy-based framework to approximate the flow velocity distribution in free-surface flows was derived by Chiu (1987, 1988) as a means to reconstruct the flow discharge based on a few velocity samples. The approach consists in expressing the spatial velocity distribution across a river cross-section as an equivalent cumulative probability distribution function, which can be determined analytically by means of the principle of maximum entropy. Unlike the logarithmic or power-function velocity profiles deriving from boundary layer theory, which are inherently one-dimensional and monotonic, the entropy approach considers the velocity distribution across the whole cross-section and allows a maximum of the velocity beneath the water surface (the so-called velocity dip). The main assumption is that the 'local' velocity maximum, $U_{\max,i} = \max_z\{U_i^{\mathrm{ent}}(z)\}$ (e.g., the maximum with respect to the vertical co-ordinate z measured at a location with horizontal co-ordinate $y_i = i\Delta y$, which we represent as discrete without loss of generality), increases monotonically with y_i from both banks to a single 'global' velocity maximum, $U_{\max} = \max_i\{U_{\max,i}\}$. Under this assumption, the non-dimensional velocity distribution along the vertical axis at the maximum velocity location can be determined analytically as a function of a single entropy parameter, M, which is linked to the ratio between the mean and maximum flow velocities, U_{mean} and $U_{\max}$, respectively (Chiu 1989):

$$\phi(M) = \frac{U_{\mathrm{mean}}}{U_{\max}} = \left(\frac{e^M}{e^M - 1} - \frac{1}{M}\right). \tag{7}$$

In the context of the present work, the main advantage of the entropy theory is its capability to express the overall velocity (and depth) distribution in a physically meaningful way as a function of a limited number of parameters, specifically, in terms of a constant ratio between local maximum and average velocities. The velocity profile $U_i^{\mathrm{ent}}(z)$ at a generic i-th location along the transect can be assumed to be similar to the one at the location of maximum velocity (Moramarco et al. 2004):

$$U_i^{\mathrm{ent}}(z) = \frac{U_{\max,i}}{M} \ln\left[1 + \left(e^M - 1\right)\frac{D_i + z}{D_i - h_i}\exp\left(1 - \frac{D_i + z}{D_i - h_i}\right)\right] \tag{8}$$

where h_i is the dip depth, i.e., the depth of $U_{\max,i}$ below the water surface. $U_{\max,i}$, and h_i are linked to M via

$$h_i = D_i - (D_i/\delta_i) \tag{9}$$

and (Fulton and Ostrowski 2008)

$$U_{\max,i} = V_i M \left[\ln\left(1 + \left(e^M - 1\right)\delta_i \exp\left(1 - \delta_i\right)\right)\right]^{-1}, \tag{10}$$

where δ_i is a so-called dip-correction factor, which can be estimated based on an empirical relation (Yang et al. 2004) as

$$\delta_i = 1 + 1.3\exp\left(-\left|y_i - y_b\right|/D_i\right), \tag{11}$$

where $|y_i - y_b|$ is the distance from y_i to the nearest bank with co-ordinate y_b.

The entropy framework can also be used to describe the variation of the water depth along a transect, D_i^{ent}, by expressing it similarly in terms of a cumulative probability distribution (Moramarco et al. 2013). As for the velocity distribution, the main assumption is that the water depth increases monotonically from both banks to a single location of maximum depth $D_{\max}$, which coincides with the location of maximum velocity $U_{\max}$. By setting the local value of the cumulative probability equal to the ratio between local surface velocity and maximum velocity, $V_i/U_{\max}$, one finds (Moramarco et al. 2013)

$$D_i^{\mathrm{ent}} = \frac{D_{\max}}{\psi}\ln\left[1 + \left(e^{\psi} - 1\right)\frac{V_i}{U_{\max}}\right], \tag{12}$$

where ψ is a second entropy parameter which depends on the ratio between the mean and the maximum depth across the transect, D_{mean} and D_{max}, respectively:

$$\frac{D_{\mathrm{mean}}}{D_{\mathrm{max}}} = \frac{e^{\psi}}{e^{\psi}-1} - \frac{1}{\psi}. \tag{13}$$

Equation (12) indicates a direct link between the non-dimensionalised surface velocity distribution, V_i/U_{max}, and the water depth distribution, $D_i^{\mathrm{ent}}/D_{\mathrm{max}}$. Modifying the two parameters D_{mean} and ψ leads to a global rescaling and smoothing or sharpening of the depth distribution, respectively. In fact, D_{max} depends linearly on D_{mean} through Eq. (13). The parameter ψ, instead, represents the strength of the depth-velocity link, such that when $\psi \to 0$, the depth distribution becomes independent of V_i and the cross section tends to a rectangular shape.

2.4. *Extended IWV approach*

As a first step, we derive a simple spatially-resolved extension of the spatially-averaged IWV approach introduced by Dolcetti et al. (2022). Assuming that the velocity and depth vary in space along the transverse co-ordinate y_i, let $D_i = D(y_i)$ and $V_i = V(y_i)$ indicate the local values of the water depth and surface velocity, and let I_i be the spectrum of a smaller portion of image with size L_i and with centre at the transverse co-ordinate y_i, the corresponding NSP_i is

$$\begin{aligned}\mathrm{NSP}_i(I_i, V_i, D_i) = &\left|\sum_{p,q,n} I_i(k_{x,p}, k_{y,q}, f_n) S(k_{x,p}, k_{y,q}, f_n, V_i, D_i)\right| \\ &\times \left|\sum_{p,q,n} I_i(k_{x,p}, k_{y,q}, f_n)\right|^{-1} \left|\sum_{p,q,n} S(k_{x,p}, k_{y,q}, f_n, V_i, D_i)\right|^{-1}.\end{aligned} \tag{14}$$

The estimated local depth D_i^{IWV} and velocity V_i^{IWV} can be calculated by applying the standard IWV analysis to this smaller image portion (window), i.e., looking for the maximum of NSP_i. Then, the velocity and depth distribution along the transect can be found by 'sliding' the window, i.e., changing the value of the index i. The final result is a distribution of surface velocity, V_i^{IWV}, and depth, D_i^{IWV}, which can be combined to provide a refined estimate of the flow discharge,

$$Q^{\mathrm{IWV}} = \alpha \Delta y \sum_i D_i^{\mathrm{IWV}} V_i^{\mathrm{IWV}}, \tag{15}$$

where $\Delta y = y_{i+1} - y_i$ identifies the spatial separation between consecutive discrete locations along the transect.

2.5. *Combined IWV-Entropy approach*

With the standard IWV approach, the calculation of the Fourier spectra is preceded by a pre-processing step and followed by a trimming and interpolation step to identify and remove potential outliers (Fig. 2a). These steps are illustrated in more detail in the following sections based on an example with real data. Here we propose an alternative combined IWV-Entropy approach, where the standard "Optimisation" step is replaced by three separate steps: Initialisation, Optimisation, and Expansion (Fig. 2b).

The first step ("Initialisation") is optional. Its role is to facilitate and accelerate the convergence of the subsequent optimisation step. This is achieved by calculating an initial approximate surface velocity distribution using the extended procedure (Section 2.4), but neglecting the depth dependence by taking the infinite-depth limit of Eq. 4. As with the standard approach, the initialised raw distribution, $V_i^{\mathrm{raw},\,\infty}$, can be refined by trimming and interpolation. The resulting distribution is identified with $V_i^{\mathrm{IWV},\infty}$ and corresponds to an initial approximation of the surface velocity distribution. Then, the search range of the following optimisation step is set to within $\pm 20\%$ of $V_i^{\mathrm{IWV},\infty}$, to speed up and facilitate the convergence.

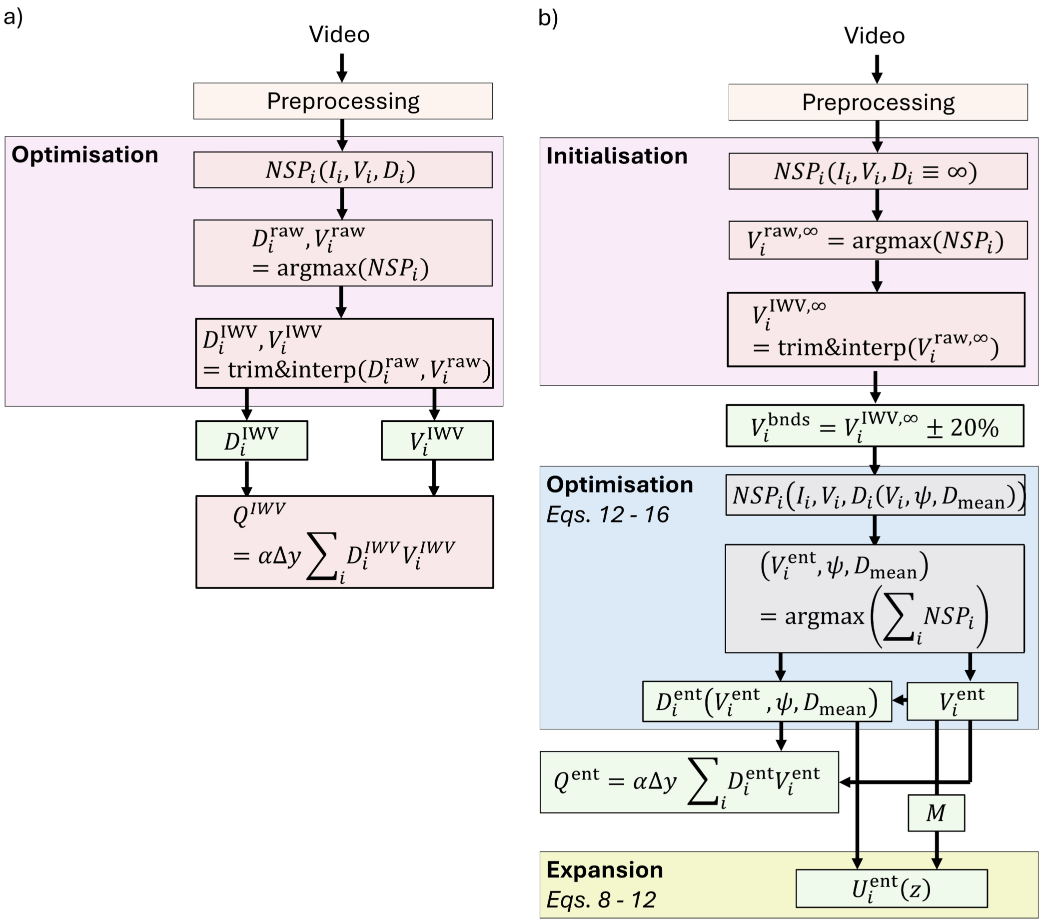

Figure 2. Schematic of the new measurement approaches: extended IWV algorithm (a) and combined IWV-entropy approach (b).

For the second step ("Optimisation"), the depth dependence is reinstated, but rather than estimating D_i separately at each location, D_i is calculated by means of the entropy theory (Eq. (12)) as a function of the surface velocity distribution V_i and of the two parameters ψ and D_{mean}. These parameters are unknown, but unlike D_i, they are "global", in the sense that a single ψ and D_{mean} pair applies at all locations along the transect, allowing a significant reduction in the number of parameters that need to be estimated. In fact, ψ, D_{mean}, and the surface velocity distribution V_i^{ent} can be estimated simultaneously by maximising a combined normalised scalar product, defined as

$$\mathrm{NSP} = \sum_i \mathrm{NSP}_i \left(I_i, V_i^{\mathrm{ent}}, D_i^{\mathrm{ent}} \left(V_i^{\mathrm{ent}}, \psi, D_{\mathrm{mean}} \right) \right). \tag{16}$$

This step results in an estimate of the surface velocity distribution, V_i^{ent}, and entropy parameters, ψ and D_{mean}. These can be employed to calculate the depth distribution D_i^{ent} using Eq. (12), and then the discharge

$$Q^{\mathrm{ent}} = \alpha \Delta y \sum_i D_i^{\mathrm{ent}} V_i^{\mathrm{ent}}. \tag{17}$$

As a third and final step ("Expansion") the velocity distribution beneath the water surface $U_i^{\mathrm{ent}}(z)$ can be reconstructed based on the entropy theory (Eq. 12) across the whole river cross-section, using the estimated surface velocity, V_i^{ent} , and depth distributions, D_i^{ent} , as input. To this end, the unknown parameter M can be calculated directly by means of Eq. (7) as a function of the cross-section-averaged velocity,

$$U_{\mathrm{mean}} = Q^{\mathrm{ent}} \left(\Delta y \sum_i D_i^{\mathrm{ent}} \right)^{-1}. \tag{18}$$

Note that this last step does not impact the calculation of the discharge since the section-averaged velocity remains the same. However, the estimation of the full velocity distribution across the cross-section can be useful to understand the interaction of the flow with the bed morphology, and to compare with direct measurements, as exemplified in Section 3.

3. Results

3.1. *Video acquisition and preprocessing*

An 80-second-long video of the water surface was recorded using a Sony FDR-AX53 camera, with 1440×1080 pixel frame size and a frame rate of 25 fps. The camera was installed onto a pole at a height of approximately 3 m above the water surface, on the left bank. The pole was held manually, and the effects of pole and camera oscillations were removed in post-processing using the open-access software Blender 4.2. Real-world coordinates of six markers distributed along both banks were measured using a Leika TCR705 total station. The markers were used as references to ortho-rectify each image (i.e., to remove perspective distortion) using the open-access LSPIV software Fudaa-LSPIV (Le Coz et al. 2014). The resulting orthorectified images had a spatial resolution of 0.01 m/pixel. The whole video was split temporally into a set of 10-second-long segments, with 50 % overlap. The rectified videos were also split spatially into a set of rectangular windows with dimensions of 1 m$\times$0.5 m (100$\times$50 pixels) along the streamwise and transverse direction, respectively. The rectangular shape of the windows allows a higher spectral resolution in the streamwise direction, while minimising the error due to the transverse variability of the flow velocity (Dolcetti et al. 2022). The windows were arranged equidistantly along the transect, with a transverse

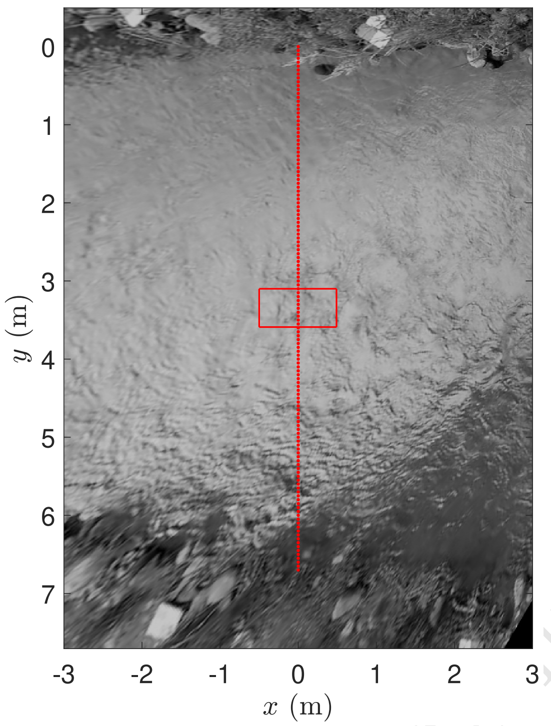

Figure 3. Example of ortho-rectified input image. The red dots indicate the measurement locations along the transect. The rectangle indicates the dimensions of a single window. The flow was from left to right.

centre-to-centre distance of 0.10 m (80 % overlap), resulting in a set of 67 transect grid points: y_i, $i = 1, \ldots, 67$ (Fig. 3).

3.2. *Extended IWV approach*

The IWV analysis was conducted using the library *kOmega* (Dolcetti et al. 2023) in Matlab. As a pre-processing step, the time series of the image intensity at each pixel were detrended and normalised based on the local standard deviation. The space-time Fourier spectra computed separately for each window were averaged across all time segments, normalised, and the noise floor below a fixed threshold was removed. These steps are performed automatically in *kOmega* (Dolcetti et al. 2023). The spectra show clear evidence of both turbulence-forced patterns and gravity-capillary waves following Eq. (1) and (4), respectively (Fig. 4).

For the analysis, the vertical velocity gradient m was set as $m = 0.3$, which corresponds to a mean-velocity-to-surface-velocity index $\alpha = 0.85$ (Eq. (6)). This value is widely regarded as a reasonable approximation in most rivers (Hauet et al. 2018). The choice of m can significantly impact the velocity and especially depth estimation with the IWV method (Dolcetti et al. 2022). The whole analysis was repeated with $\alpha = 0.8$ ($m = 0.4$) and $\alpha = 0.9$ ($m = 0.2$) to quantify the impact of m on the results.

With the extended IWV approach, the best-fit flow velocity and depth were searched for within finite intervals of 0 to 1 m/s for the streamwise velocity, -0.2 to 0.2 m/s for the transverse velocity, and 0.01 to 1 m for the water depth. Ten runs of the optimisation were conducted for each window to identify the absolute optimum among potential local maxima of the normalised scalar product. The estimated surface velocity and depth distributions were indicated as V_i^{raw} and D_i^{raw}, respectively (Fig. 5a

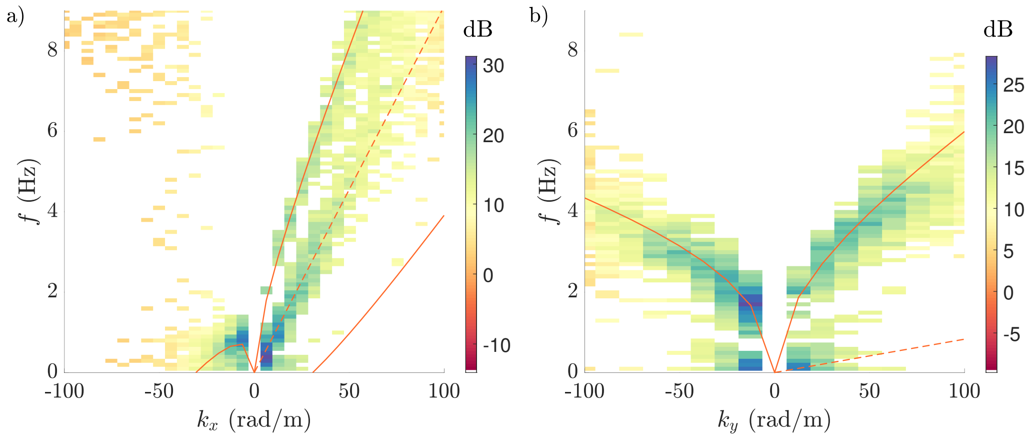

Figure 4. Example of normalised measured frequency-wavenumber spectra of the water surface images projected along the streamwise (a) and transverse (b) directions. The red lines indicate the wavenumber-frequency relations of turbulence-forced patterns (dashed, Eq. 1) and gravity-capillary waves (solid, Eq. 4), respectively.

and b).

Unexpectedly large velocity estimates were observed within a distance of approximately 0.5 m from the banks, where the velocity should have been decreasing to zero. These large velocities were likely an artefact due to the reflections of the banks and vegetation on water (see Fig. 3). Depth estimations showed a significant scatter across the whole transect and some very large (> 0.5 m) or very small (≈ 0 m) values, especially near the centre of the channel (Fig. 5b). These are indicative of the lack of robustness of depth estimates by the IWV method when the window size is relatively small. To reduce the impact of these erroneous velocity and depth estimates on the calculation of the discharge, all data (velocity and depth) within a distance of 0.5 m from the banks and all depth data deviating from the average depth by more than 50 % were discarded, and replaced by a linear interpolation between the remaining valid data points. The resulting surface velocity and depth distributions were indicated as V_i^{IWV} and D_i^{IWV}, respectively.

The variation of V_i^{IWV} and D_i^{IWV} with α is represented by the shaded area in Fig. 5a and b, respectively. The estimated velocity distributions had a minimal variation when α varied between 0.8 and 0.9. In turn, the estimated depth values changed by up to 10 cm, or 30 % of the average water depth. Larger depths were estimated assuming $\alpha = 0.9$. Direct measurements of the surface velocity were not available since the instrument could not measure within 7 cm from the surface. Depth estimations by the extended IWV approach (Fig. 5b) showed a good agreement with direct measurements, but only after the removal of the outliers near the centre of the channel and banks. The discharge calculated with the extended IWV approach (Eq. 15) assuming $\alpha = 0.85$ was $Q^{\mathrm{IWV}} = 0.90$ m^3/s (0.83 m^3/s if $\alpha = 0.80$ and 1.12 m^3/s if $\alpha = 0.90$). This compared reasonably well with the direct measurement of $Q = 1.0$ m^3/s.

3.3. *Combined IWV-entropy analysis*

Velocity distributions calculated with the combined IWV-entropy approach (V^{ent}) are very similar to those obtained with the extended method (V^{IWV}) (Fig. 6a). This was expected, since the entropy theory affects the calculations of the surface velocity only indirectly through changes in the depth distribution, and depth variations have a

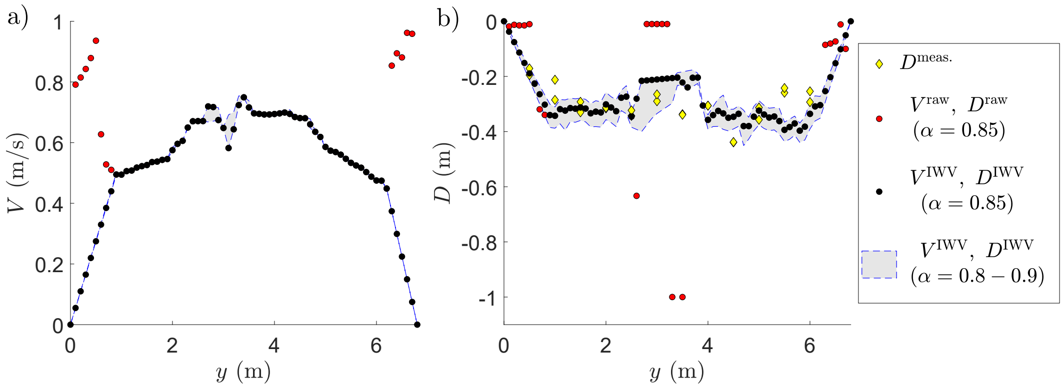

Figure 5. Velocity (a) and depth (b) estimation based on the standard IWV approach. V^{raw} and D^{raw} outliers (red circles) near the banks and the centre of the channel are removed and replaced by a linear interpolation between valid points to obtain the final estimates V^{IWV} and D^{IWV} (black circles). Results indicated with circles were obtained assuming $\alpha = 0.85$. The shaded region indicates the variation in V^{ent} and D^{ent} when the velocity index α changed between 0.80 and 0.90. Direct depth measurements $D^{\text{meas.}}$ are shown for comparison (yellow).

small impact on the estimated velocity. The impact was appreciable, however, near the centre of the channel, where the smoother depth reconstruction using the entropy approach (Fig. 6b) yields a smoother distribution of V^{ent} compared to V^{IWV} (Fig. 6a). In the same region, V^{IWV} and V^{ent} differed slightly also in terms of their directions (Fig. 7). As noted previously, changes in α had a very small effect on the estimated surface velocity distributions.

The difference between the extended IWV approach and the combined IWV-entropy approaches becomes clearer when looking at the reconstructed bathymetries (Fig. 5b, Fig. 6b). The reconstruction with the combined method, D_i^{ent} (Fig. 6b) is significantly smoother than D_i^{IWV}. Both reconstructions are in good agreement with direct measurements, although the combined-method estimates appear to be more accurate near the centre of the channel, where the extended-method results had to be interpolated. Near the banks, instead, the combined approach appears to overestimate the water depth. Different choices of the parameter α (and m) had a significant impact on the average water depth estimated with the combined approach, which varied from 0.28 m ($\alpha = 0.80$) to 0.34 m ($\alpha = 0.90$). The average water depth when $\alpha = 0.85$ was 0.30 m.

3.4. *Vertical velocity distributions*

As a last step, the velocity distribution over the whole cross-section, $U_i^{\text{ent}}(z)$ (Figure 8), was calculated based on the entropy theory (Eq. (8)) using the bathymetry and surface velocity distribution estimated with the combined method (D_i^{ent} and V^{ent}, respectively). The entropy parameter M was calibrated by matching the average of $U_i^{\text{ent}}(z)$ over the entire cross-section with the average based on the linear velocity profile according to Eq. (18).

The reconstruction of the whole velocity distribution based on the entropy theory enables a direct comparison with the measured velocity profiles (Fig. 9). The velocity profiles predicted by Eq. (8) were generally in good agreement with the measurements, confirming the validity of the theory. The estimations based on $\alpha = 0.85$ approximated the measurements more closely, especially in terms of water depth distribution. The

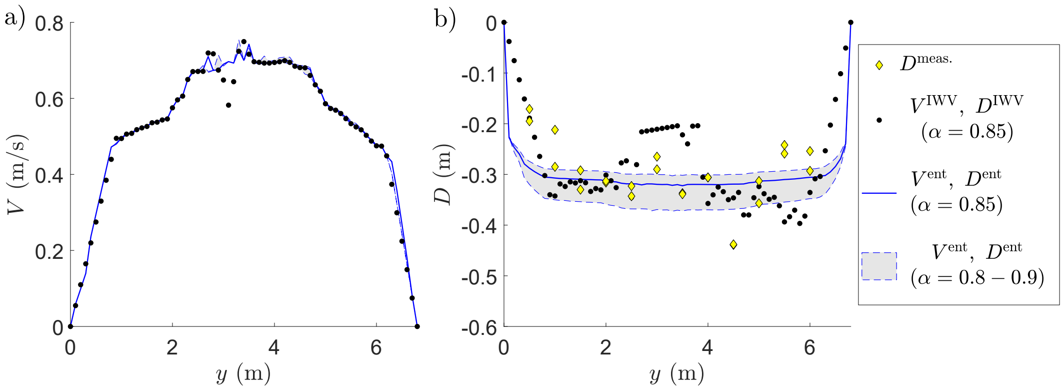

Figure 6. Velocity (a) and depth (b) reconstruction obtained with the combined IWV-entropy approach (blue line) (V^{ent} and D^{ent}, respectively) compared with those obtained with the extended approach (black circles) (V^{IWV} and D^{IWV}, respectively). The direct comparison is limited to the calculations obtained with $\alpha = 0.85$. The shaded region indicates the variation in V^{ent} and D^{ent} when the velocity index α changed between 0.80 and 0.90. Direct depth measurements $D^{\text{meas.}}$ are shown for comparison.

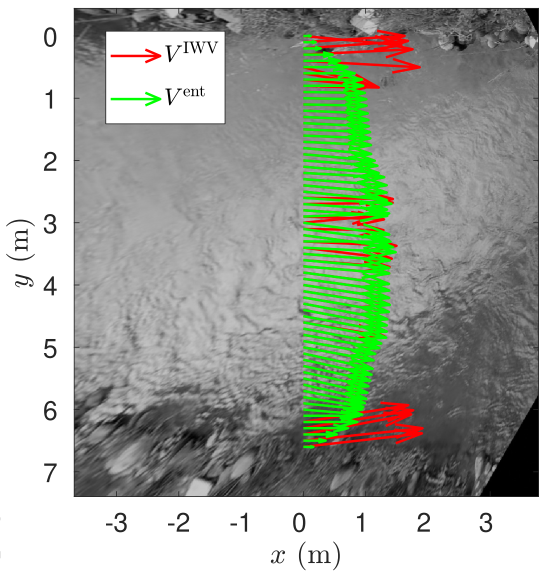

Figure 7. Velocity vectors reconstruction based on the extended IWV approach (red) and the combined IWV-entropy approach (green). The velocity vectors have been scaled by a factor of 2 to improve the visualisation.

comparison shows a good resemblance between measurements and estimations in the central sections of the river (1.5 m $\leq y \leq$ 4.0 m), where velocity magnitudes were larger. Larger discrepancies near the banks ($y \leq 1$ m and $y \geq 5$ m) are attributed to the effects of reflections in the videos and the consequent outliers removal and linear interpolation.

3.5. *Discharge calculation and uncertainties*

The discharge estimations based on the extended IWV and combined IWV-entropy approach are summarised in Table 1 along with the estimated entropy parameters ψ, D_m, and M. The discharge estimated with the combined IWV-entropy approach

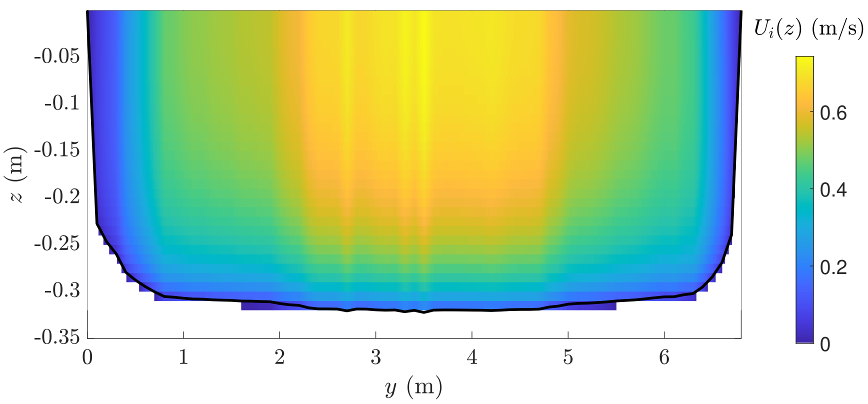

Figure 8. Cross-sectional distribution of the velocity estimated with the combined IWV-entropy approach. The black line indicates the reconstructed bathymetry.

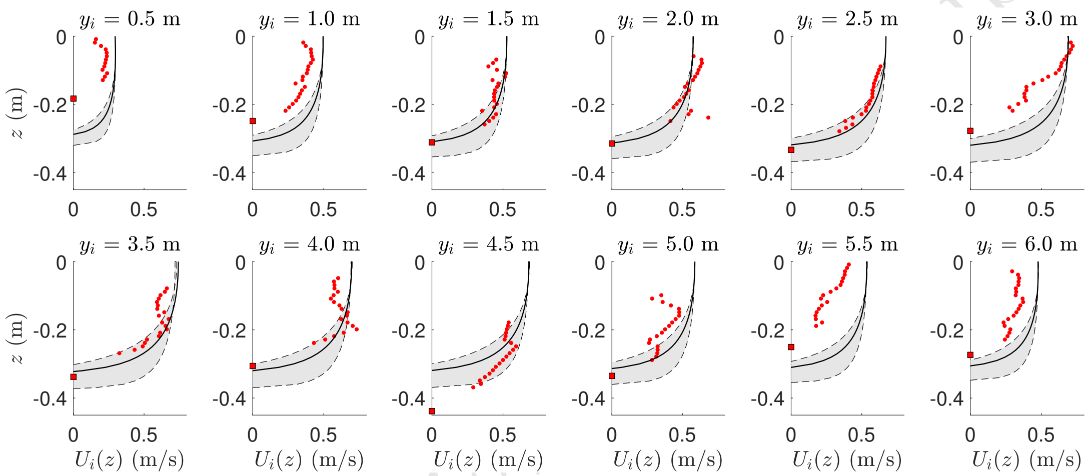

Figure 9. Comparison between measured and estimated velocity profiles at each measurement location along the transect (y between 0.5 m and 6.0 m). The measured velocities (red circles) are the average of two distinct rounds of measurements. The solid black line indicates the predictions by the combined IWV-entropy method assuming $\alpha = 0.85$. The shaded region indicates the range of variability in the velocity profiles when α varied between 0.8 (upper boundary of the region) and 0.9 (lower boundary).

was 4 to 7 % higher than the estimate obtained with the extended IWV method, but still 4 % lower than the direct measurement of 1.0 m^3/s obtained with the intrusive instrumentation. Considering that both estimates were obtained fully remotely, and with a faster and significantly less expensive setup than the direct measurements, the accuracy was deemed satisfactory.

In terms of the entropy parameters (Table 1), increasing α led to a decrease in ψ and an increase in M. The decrease in ψ indicates less sensitivity of the estimated depth distribution from the velocity distribution, and a tendency towards a rectangular channel cross-section, which could lead to a larger section area and a further increase in discharge. For a fixed maximum surface velocity, the increase in M is associated with an increase in mean velocity U_{mean}, which also contributes to an increase in discharge. While the entropy-based full cross-sectional distribution of the velocity allows for a direct calculation of the discharge without explicitly including the factor α, this distribution is affected by the choice of α indirectly due to the effects on the intermediate IWV step results.

While a value of $\alpha = 0.85$ can be reasonably assumed in most occasions, the choice

Table 1. Estimated discharge and entropy parameters assuming different values of the velocity index α.

	$\alpha = 0.85$	$\alpha = 0.80$	$\alpha = 0.90$
Q^{IWV} ($\mathrm{m^3/s}$)	0.90	0.83	1.12
Q^{ent} ($\mathrm{m^3/s}$)	0.96	0.86	1.16
ψ	8.60	10.0	6.35
D_m(m)	0.28	0.27	0.31
M	2.63	1.38	4.53

of the velocity index remains one of the main sources of uncertainty for discharge estimates based on non-contact velocimetry approaches (Hauet et al. 2018). With traditional non-contact methods, the dependence of the discharge on α is linear. With the IWV method, however, the uncertainty is amplified by the fact that α also affects the estimated velocity and depth according to Eq. (4)-(6) (Dolcetti et al. 2022). Here, varying the velocity index α between 0.80 and 0.90 (± 12 %) resulted in a slightly amplified relative variation (± 15 %) in estimated discharge with both the extended and combined approach. From this point of view, the integration in the entropy framework appears to have a limited impact on the measurement uncertainties.

4. Conclusions

We derived and validated two novel approaches to simultaneously reconstruct the spatial distribution of the flow velocity and water depth along a river transect, based solely on the non-contact imaging of water surface dynamics. The first approach, a simple spatially-resolved extension of the previous spatially averaged approach introduced by Dolcetti et al. (2020), shows large local errors in the depth reconstruction, indicative of a lack of robustness. The estimated discharge in a test case study was 10 % smaller than the direct measurement. The second approach combines the IWV method with the entropy theory to limit the spatial variability of the estimated bathymetry using a set of theoretical constraints that ensure the physical admissibility of the reconstructions. The bathymetry reconstruction obtained with the combined method was found to be more robust due to the smaller number of free parameters and to the control exerted by the estimated velocity distribution, which can be determined more accurately and with a higher resolution. The estimated discharge with the combined measurement was 4 % smaller than the direct measurement, which included the effects of imaging errors due to reflection and shadows of the banks on the water surface. The method has the additional advantage of enabling the reconstruction of a physically admissible velocity distribution over the entire two-dimensional river cross-section, which is beyond the capabilities of other existing non-contact velocimetry approaches. This capability could pave the way for the remote characterisation of the bed morphodynamic evolution and of the interaction of the flow with engineering structures.

Both measurement approaches introduced here show a clear potential to address two key challenges of non-contact discharge measurements in rivers: the need for a high density of passive tracers, and the need for prior knowledge of the bathymetry. Compared to alternative fully non-contact approaches (Legleiter and Kinzel 2021, Chen et al. 2023), they do not require an on-site calibration or the knowledge of additional parameters, except the velocity index, which is confirmed as the key term governing the uncertainties of any non-contact velocimetry technique. The methods were validated at a test site where the Froude number based on the averaged velocity and depth was approximately 0.3. This is lower than the range of previous validations of the standard IWV approach (Dolcetti et al. 2022, 2024a), but it is still indicative of a relatively shallow and fast flow. The depth reconstruction by the IWV approach has a very low sensitivity in deep flows, and it relies on water surface deformations, which typically become visible when the Froude number is at least of order $\mathcal{O}(0.1)$. For sufficiently shallow and deep flows, the proposed methodology provides a robust, rapid, low-cost, and fully non-contact alternative to traditional and more advanced flow measurement approaches, creating unprecedented opportunities for monitoring rivers and/or flow conditions beyond state-of-the-art measurement capabilities.

Funding details

The work of G. Dolcetti was financed by the European Union - Next Generation EU, Mission 4 Component 2 - CUP 20222W5WXC.

Credit authorship contribution Statement

Giulio Dolcetti: Investigation, Methodology, Formal Analysis, Data collection, Writing - Original Draft, Visualization.

Farhad Bahmanpouri: Investigation, Methodology, Formal Analysis, Writing - Original Draft.

Ashkan Pilbala: Investigation, Methodology, Formal Analysis, Data collection, Writing - Original Draft, Visualization.

Declaration of Interests

The authors report no conflict of interest.

Data availability

All data and codes used for this work are openly available at the following link (Dolcetti et al. 2025): `https://doi.org/10.5281/zenodo.15804179`.

References

Alimenti, F., Bonafoni, S., Gallo, E., Palazzi, V., Gatti, R. V., Mezzanotte, P., Roselli, L., Zito, D., Barbetta, S., Corradini, C., et al. (2020). Noncontact measurement of river surface velocity and discharge estimation with a low-cost Doppler radar sensor. *IEEE Transactions on Geoscience and Remote Sensing*, 58(7):5195–5207.

Almar, R., Bergsma, E. W., Catalan, P. A., Cienfuegos, R., Suarez, L., Lucero, F., Lerma, A. N., Desmazes, F., Perugini, E., Palmsten, M. L., et al. (2021). Sea state from single optical images: A methodology to derive wind-generated ocean waves from cameras, drones and satellites. *Remote Sensing*, 13(4):679.

Bahmanpouri, F., Barbetta, S., Gualtieri, C., Ianniruberto, M., Filizola, N., Termini, D., and Moramarco, T. (2022a). Prediction of river discharges at confluences based on entropy theory and surface-velocity measurements. *Journal of Hydrology*, 606:127404.

Bahmanpouri, F., Eltner, A., Barbetta, S., Bertalan, L., and Moramarco, T. (2022b). Estimating the average river cross-section velocity by observing only one surface velocity value and calibrating the entropic parameter. *Water Resources Research*, 58(10):e2021WR031821.

Benetazzo, A., Gamba, M., and Barbariol, F. (2017). Unseeded large scale PIV measurements corrected for the capillary-gravity wave dynamics. *Rendiconti Lincei*, 28:393–404.

Biesel, F. (1950). Etude théorique de la houle en eau courante. *La Houille Blanche*, pages 279–285.

Brocchini, M. and Peregrine, D. H. (2001). The dynamics of strong turbulence at free surfaces. Part 1. Description. *Journal of Fluid Mechanics*, 449:225–254.

Chen, Z., Wang, T., Zhao, C., and He, Z. (2023). River discharge inversion algorithm based on the surface velocity of microwave Doppler radar. *Remote Sensing*, 15(19):4727.

Chiu, C.-L. (1987). Entropy and probability concepts in hydraulics. *Journal of Hydraulic Engineering*, 113(5):583–599.

Chiu, C.-L. (1988). Entropy and 2-D velocity distribution in open channels. *Journal of Hydraulic Engineering*, 114(7):738–756.

Chiu, C.-L. (1989). Velocity distribution in open channel flow. *Journal of Hydraulic Engineering*, 115(5):576–594.

Dal Sasso, S. F., Pizarro, A., and Manfreda, S. (2020). Metrics for the quantification of seeding characteristics to enhance image velocimetry performance in rivers. *Remote Sensing*, 12(11):1789.

Dal Sasso, S. F., Pizarro, A., Samela, C., Mita, L., and Manfreda, S. (2018). Exploring the optimal experimental setup for surface flow velocity measurements using PTV. *Environmental Monitoring and Assessment*, 190:1–14.

Dolcetti, G., Bahmanpouri, F., and Pilbala, A. (2025). Supplementary data and software for "Fully non-contact discharge measurement in shallow streams via physics-based water-surface image analysis. `https://doi.org/10.5281/zenodo.15804179`.

Dolcetti, G. and García Nava, H. (2019). Wavelet spectral analysis of the free surface of turbulent flows. *Journal of Hydraulic Research*, 57(2):211–226.

Dolcetti, G., Horoshenkov, K. V., Krynkin, A., and Tait, S. J. (2016). Frequency-wavenumber spectrum of the free surface of shallow turbulent flows over a rough boundary. *Physics of Fluids*, 28(10).

Dolcetti, G., Hortobágyi, B., Perks, M., and Tait, S. J. (2020). The effect of surface gravity waves on the measurement of river surface velocity. *River Flow 2020*, pages 862–871.

Dolcetti, G., Hortobágyi, B., Perks, M., and Tait, S. J. (2023). kOmega-a Matlab script to estimate river discharge remotely based on water surface dynamics. `https://doi.org/10.5281/zenodo.7998890`.

Dolcetti, G., Hortobágyi, B., Perks, M., Tait, S. J., and Dervilis, N. (2022). Using noncontact measurement of water surface dynamics to estimate river discharge. *Water Resources Research*, 58(9):e2022WR032829.

Dolcetti, G. and Krynkin, A. (2017). Doppler spectra of airborne ultrasound forward scattered by the rough surface of open channel turbulent water flows. *The Journal of the Acoustical Society of America*, 142(5):3122–3134.

Dolcetti, G., Krynkin, A., Alkmim, M., Cuenca, J., De Ryck, L., Sailor, G., Muraro, F., Tait, S. J., and Horoshenkov, K. V. (2024a). Reconstruction of the frequency-wavenumber spectrum of water waves with an airborne acoustic Doppler array for noncontact river monitoring. *IEEE Transactions on Geoscience and Remote Sensing*, 62:1–14.

Dolcetti, G., Krynkin, A., and Horoshenkov, K. V. (2017). Doppler spectra of airborne sound backscattered by the free surface of a shallow turbulent water flow. *The Journal of the Acoustical Society of America*, 142(6):3387–3401.

Dolcetti, G., Winsemius, H., and Peña Haro, S. (2024b). IWaVE: Image-based Water surface Velocimetry and Elevation. `https://pypi.org/project/iwave/`. Accessed: 2025-06-26.

Fujita, I., Muste, M., and Kruger, A. (1998). Large-scale particle image velocimetry for flow analysis in hydraulic engineering applications. *Journal of Hydraulic Research*, 36(3):397–414.

Fujita, I. and Tsubaki, R. (2002). A novel free-surface velocity measurement method using spatio-temporal images. In *Hydraulic Measurements and Experimental Methods 2002*, pages 1–7.

Fulton, J. and Ostrowski, J. (2008). Measuring real-time streamflow using emerging technologies: Radar, hydroacoustics, and the probability concept. *Journal of Hydrology*, 357(1-2):1–10.

Hauet, A., Kruger, A., Krajewski, W. F., Bradley, A., Muste, M., Creutin, J.-D., and Wilson, M. (2008). Experimental system for real-time discharge estimation using an image-based method. *Journal of Hydrologic Engineering*, 13(2):105–110.

Hauet, A., Morlot, T., and Daubagnan, L. (2018). Velocity profile and depth-averaged to surface velocity in natural streams: A review over a large sample of rivers. In *E3s Web of Conferences*, volume 40, page 06015. EDP Sciences.

Jolley, M. J., Russell, A. J., Quinn, P. F., and Perks, M. T. (2021). Considerations when applying large-scale piv and ptv for determining river flow velocity. *Frontiers in Water*, 3:709269.

Kechnit, D., Tshimanga, R. M., Ammari, A., Trigg, M. A., Carr, A. B., Bahmanpouri, F., Barbetta, S., and Moramarco, T. (2024). Bathymetry and discharge estimation in large and data-scarce rivers using an entropy-based approach. *Hydrological Sciences Journal*, 69(15):2109–2123.

Khalid, M., Pénard, L., and Mémin, E. (2019). Optical flow for image-based river velocity estimation. *Flow Measurement and Instrumentation*, 65:110–121.

Le Coz, J., Jodeau, M., Hauet, A., Marchand, B., and Le Boursicaud, R. (2014). Image-based velocity and discharge measurements in field and laboratory river engineering studies using the free FUDAA-LSPIV software. In *River Flow*, volume 2014, pages 1961–1967. Lausanne Switzerland.

Legleiter, C. and Kinzel, P. (2021). Depths inferred from velocities estimated by remote sensing: A flow resistance equation-based approach to mapping multiple river attributes at the reach scale. *Remote Sensing*, 13(22):4566.

Legleiter, C. J., Kinzel, P. J., Engel, F. L., Harrison, L. R., and Hewitt, G. (2024). A two-dimensional, reach-scale implementation of space-time image velocimetry (STIV) and comparison to particle image velocimetry (PIV). *Earth Surface Processes and Landforms*, 49(10):3093–3114.

Ljubičić, R., Dal Sasso, S. F., and Zindović, B. (2024). SSIMS-Flow: Image velocimetry workbench for open-channel flow rate estimation. *Environmental Modelling & Software*, 173:105938.

Manfreda, S., Miglino, D., Saddi, K. C., Jomaa, S., Eltner, A., Perks, M., Peña-Haro, S., Bogaard, T., van Emmerik, T. H., Mariani, S., et al. (2024). Advancing river monitoring using image-based techniques: Challenges and opportunities. *Hydrological Sciences Journal*, 69(6):657–677.

Miles, J. W. (1957). On the generation of surface waves by shear flows. *Journal of Fluid Mechanics*, 3(2):185–204.

Moramarco, T., Corato, G., Melone, F., and Singh, V. P. (2013). An entropy-based method for determining the flow depth distribution in natural channels. *Journal of Hydrology*, 497:176–188.

Moramarco, T., Saltalippi, C., and Singh, V. P. (2004). Estimation of mean velocity in natural channels based on Chiu's velocity distribution equation. *Journal of Hydrologic Engineering*, 9(1):42–50.

Muraro, F., Dolcetti, G., Nichols, A., Tait, S. J., and Horoshenkov, K. V. (2021). Free-surface behaviour of shallow turbulent flows. *Journal of Hydraulic Research*, 59(1):1–20.

Peña-Haro, S., Carrel, M., Lüthi, B., Hansen, I., and Lukes, R. (2021). Robust image-based streamflow measurements for real-time continuous monitoring. *Frontiers in Water*, 3:766918.

Perks, M. T. (2020). KLT-IV v1. 0: Image velocimetry software for use with fixed and mobile platforms. *Geoscientific Model Development Discussions*, 2020:1–27.

Phillips, O. M. (1957). On the generation of waves by turbulent wind. *Journal of Fluid*

Mechanics, 2(5):417–445.

Plant, W. J., Keller, W. C., and Hayes, K. (2005). Measurement of river surface currents with coherent microwave systems. *IEEE Transactions on Geoscience and Remote Sensing*, 43(6):1242–1257.

Rezazadeh, S., Manafpour, M., Bahmanpouri, F., and Gualtieri, C. (2025). Application of the entropy model to estimate flow discharge and bed load transport in a large river. *Physics of Fluids*, 37(2).

Senet, C. M., Seemann, J., and Ziemer, F. (2001). The near-surface current velocity determined from image sequences of the sea surface. *IEEE Transactions on Geoscience and Remote Sensing*, 39(3):492–505.

Streßer, M., Carrasco, R., and Horstmann, J. (2017). Video-based estimation of surface currents using a low-cost quadcopter. *IEEE Geoscience and Remote Sensing Letters*, 14(11):2027–2031.

Tauro, F., Piscopia, R., and Grimaldi, S. (2019). PTV-Stream: A simplified particle tracking velocimetry framework for stream surface flow monitoring. *Catena*, 172:378–386.

Tauro, F., Porfiri, M., and Grimaldi, S. (2014). Orienting the camera and firing lasers to enhance large scale particle image velocimetry for streamflow monitoring. *Water Resources Research*, 50(9):7470–7483.

Teixeira, M. A. C. and Belcher, S. E. (2006). On the initiation of surface waves by turbulent shear flow. *Dynamics of Atmospheres and Oceans*, 41(1):1–27.

Weichert, S., Smeltzer, B. K., and Ellingsen, S. Å. (2024). The effect of horizontal shear on extracting water currents from surface wave data. *IEEE Transactions on Geoscience and Remote Sensing*.

Woodget, A. S., Carbonneau, P. E., Visser, F., and Maddock, I. P. (2015). Quantifying submerged fluvial topography using hyperspatial resolution UAS imagery and structure from motion photogrammetry. *Earth Surface Processes and Landforms*, 40(1):47–64.

Yang, S.-Q., Tan, S.-K., and Lim, S.-Y. (2004). Velocity distribution and dip-phenomenon in smooth uniform open channel flows. *Journal of Hydraulic Engineering*, 130(12):1179–1186.

Young, D. S., Hart, J. K., and Martinez, K. (2015). Image analysis techniques to estimate river discharge using time-lapse cameras in remote locations. *Computers & Geosciences*, 76:1–10.

Zhao, H., Chen, H., Liu, B., Liu, W., Xu, C.-Y., Guo, S., and Wang, J. (2021). An improvement of the Space-Time Image Velocimetry combined with a new denoising method for estimating river discharge. *Flow Measurement and Instrumentation*, 77:101864.